ACS Biomaterials SCIENCE & ENGINEERING Article
Cite This: ACS Biomater. Sci. Eng. XXXX, XXX, XXX−XXX

Biomimetic Tooth Repair: Amelogenin-Derived Peptide Enables in Vitro Remineralization of Human Enamel

Sami Dogan,[†] Hanson Fong,[‡] Deniz T. Yucesoy,[‡] Timothee Cousin,[§] Carolyn Gresswell,[‡] Sefa Dag,[‡] Greg Huang,[§] and Mehmet Sarikaya*[,‡,∥,⊥]

[†]Department of Restorative Dentistry, [‡]GEMSEC, Genetically Engineered Materials Science and Engineering Center and Department of Materials Science and Engineering, [§]Department of Orthodontics, [∥]Deparment of Chemical Engineering, [⊥]Department of Oral Health Sciences, University of Washington, Seattle, Washington 98195, United States

Supporting Information

ABSTRACT: White spot lesions (WSL) and incipient caries on enamel surfaces are the earliest clinical outcomes for demineralization and caries. If left untreated, the caries can progress and may cause complex restorative procedures or even tooth extraction which destroys soft and hard tissue architecture as a consequence of connective tissue and bone loss. Current clinical practices are insufficient in treating dental caries. A long-standing practical challenge associated with demineralization related to dental diseases is incorporating a functional mineral microlayer which is fully integrated into the molecular structure of the tooth in repairing damaged enamel. This study demonstrates that small peptide domains derived from native protein amelogenin can be utilized to construct a mineral layer on damaged human enamel in vitro. Six groups were prepared to carry out remineralization on artificially created lesions on enamel: (1) no treatment, (2) Ca^{2+} and PO_4^{3-} only, (3) 1100 ppm fluoride (F), (4) 20 000 ppm F, (5) 1100 ppm F and peptide, and (6) peptide alone. While the 1100 ppm F sample (indicative of common F content of toothpaste for homecare) did not deliver F to the thinly deposited mineral layer, high F test sample (indicative of clinical varnish treatment) formed mainly CaF_2 nanoparticles on the surface. Fluoride, however, was deposited in the presence of the peptide, which also formed a thin mineral layer which was partially crystallized as fluorapatite. Among the test groups, only the peptide-alone sample resulted in remineralization of fairly thick (10 μm) dense mineralized layer containing HAp mineral, resembling the structure of the healthy enamel. The newly formed mineralized layer exhibited integration with the underlying enamel as evident by cross-sectional imaging. The peptide-guided remineralization approach sets the foundation for future development of biomimetic products and treatments for dental health care.

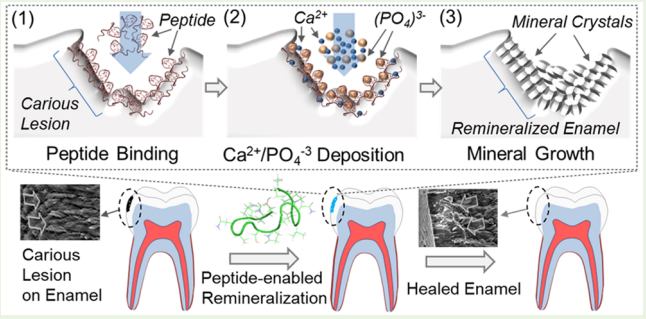

KEYWORDS: *dental remineralization, white spot lesion, demineralization, bioinformatics, molecular biomimetics, amelogenin-derived peptides*

INTRODUCTION

Dental caries is a major public health problem and a highly prevalent disease among the global population.[1] Incipient caries and white spot lesions (WSL) as well as hypersensitivity are the earliest clinical evidence of enamel demineralization and dental caries.[2] Caries forms when tooth enamel is exposed to acid produced by cariogenic bacteria. As a result, acid diffuses into surface enamel and dissolves hydroxyapatite (HAp) mineral. Due to its nonregenerative nature, enamel is unable to heal and repair itself postdemineralization.[3,4]

Traditionally, fluoride (F) has been used as the key agent in prevention of caries. Fluoride functions primarily via topical mechanisms.[5−8] It is believed that fluoride forms a thin layer of new but harder mineral, namely fluorapatite (FAp), which is incorporated into the existing HAp mineral on the tooth surface.[8] There is a trend of enhancing the remineralization effect of fluoride with calcium and phosphate supplementation in high risk individuals.[9−14] Although controversial,[15] the use of fluoride products remains the primary treatment modality for caries prevention and remineralization, with major limitations regarding the efficacy of these products for the reversal or prevention of dental caries. Fluoride delivery systems, therefore, are not sufficient to overcome the high caries risk, especially in the younger and elderly populations.[15]

Despite dental caries being a preventable infectious disease,[16] oral health promotion and prevention can fail due to many factors.[17] The advanced cavitation of the carious lesion necessitates restoring the tooth with materials such as metals, composite resins, and ceramics to replace the lost enamel or even dentin. However, modern dental materials to repair cavitated carious lesions are not compatible with biological tissues at the lesion/restorative material interface mainly

Received: December 6, 2017
Accepted: March 9, 2018
Published: March 9, 2018

DOI: 10.1021/acsbiomaterials.7b00959
ACS Biomater. Sci. Eng. XXXX, XXX, XXX−XXX

because of their physical (crystallography, morphology, property) and chemical differences (elemental compositions and phases) compared to the natural tooth structure.[18] Even though treatment of early caries lesions by the application of various types of nanosized HAp or $CaPO_4$ with or without F has received considerable attention,[19−22] their clinical validation is still lacking.[20,22] Low solubility of the calcium phosphates, particularly in the presence of fluoride ions, is the main difficulty with the clinical application of remineralization. Using biomimetic pathways, considerable attempts have been made to form a remineralized layer on the surface of enamel or dentin, or even cementum, to repair or reconstruct the lost mineral and hence restore the original structure and the resulting function.[23−30] These studies included the use of full-length amelogenin,[24,28] LRAP,[29] peptides,[26,27] dendrimers,[30] and physical chemistry approaches.[25,30] These studies contributed to the general knowledge of tooth surface remineralization; so far, however, no clinical remineralization system has emerged to promote biomimetic enamel subsurface remineralization in vivo.

A protocol was recently developed in the authors' lab to identify peptide sequences from native proteins with the potential to repair damaged dental tissues by biomimicking HAp biomineralization.[31] Using a newly developed bioinformatics scoring matrix,[32] specific peptide domains (each containing 15−40 amino acids) within (180 amino acid-long) amelogenin protein (rM180) were identified based on the similarity with a set (155 sequences) of HAp-binding peptides (HABPs) which were originally selected by 7-AA and 12-AA phage display peptide libraries.[33] Among these peptide domains, referred to as amelogenin-derived peptides (ADPs), a 22-amino acids long peptide ADP5 (see Supporting Information) was shown to facilitate cell-free and fast formation mineral layer on demineralized human root dentin. Dubbed as cementomimetic layer, the newly formed mineralized coating was found to be structurally and mechanically integrated into the underlying dentin, resembling cementum with mechanical and chemical durability providing biogenic surface for the PDL cells to attach, grow, and proliferate.[31] The ADPs in general and ADP5 in particular epitomize the unique features of the natural protein amelogenin, the key protein in enamel and cementum formation,[34−36] especially the function of capturing the constituent ions, synthesizing the mineral, and controlling its morphology on the surface and the root of the tooth.

Incorporating a functional and biomimetic mineral layer to the molecular structure of the tooth to repair damaged enamel tissue has been a long-standing challenge.[31,37] A better understanding of peptide-guided remineralization on human tooth and, therefore, the ability to control the mineral layer properties, with no, low, or high-F content, has enormous clinical implications to restore enamel and other dental hard tissues. As a major step toward this overarching goal, the objective of this study has been to develop an in vitro, cell-free, natural remineralization model on artificially induced enamel lesions. Because of the unique biomineralization characteristic and its short and simple sequence, shortened ADP5 (shADP5) was used in this research as the active ingredient in solution for the formation of mineralized layer. The work presented herein could eventually form the foundation of developing clinical products (dental gels, toothpastes, and oral-health solutions) and treatments for the restoration of early stage cavities, e.g., incipient caries, white spot lesions, and hypersensitivity.

MATERIALS AND METHODS

Sample Preparation and Test Groups. Extracted human molar teeth with no visible white spot lesions, caries, or any other kind of restorations were collected from dental clinics around the King County area (WA, United States) and disinfected in 10% aqueous bleach solutions. [Human Subject Division (University of Washington) approved the application for nonidentifiable specimen use on 04/19/2016. It should be noted that for the extracted teeth, the identification of the patients was not made and, therefore, approval from the ethical committee was not needed.] Prior to the experiments, the teeth were cleaned to remove visible blood, gross debris, and soft connective tissue using a dental scaler under a light microscope.

Formation of Artificial Lesions. Enamel was demineralized to create artificial lesions to mimic white spot lesions and/or incipient caries using a protocol modeled after previous work for creating artificial lesions[38−40] which is outlined in Figure 1. The teeth were covered by lacquer leaving a 4 mm wide square window in the enamel close to cemento−enamel junction. The exposed areas of 4 × 4 mm enamel were treated with a cocktail of acetic acid/$CaCl_2$/KH_2PO_4 for 2 weeks to establish up to 200 μm deep artificially created noncavitated WSL.[38−40] Specifically, WSL were produced by daily cycling at 37 °C between demineralization and neutral solutions for 6 and 17.5 h, respectively. Demineralization solution was made of 1.2 mM KH_2PO_4 (USB Corporation, Cleveland, OH, United States), 2.0 mM $CaCl_2$ (Johnson Matthey Inc., Seabrook, NH, United States) and 75 mM acetic acid (EMD Chemicals, Savannah, GA, United States) in deionized water at pH 4.2. Neutral solution was made of 0.9 mM KH_2PO_4 (USB Corporation, Cleveland, OH, United States), 1.5 mM $CaCl_2$, 150 mM KCl (Johnson Matthey Inc., Seabrook, NH, United States) in 20 mM Tris (EMD Chemicals, Savannah, GA, United States) buffered at pH 7.0. The demineralization solution was replaced daily. Samples were then divided into control and test groups. Test groups were treated either with peptide, fluoride, or a combination of both (Table 1).

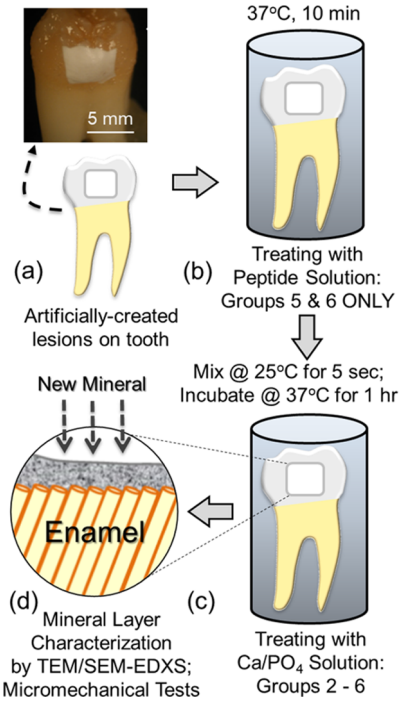

Figure 1. (a) White spot lesion was artificially created by exposing a window on the tooth surface for demineralization. (b) Group 5 and 6 samples were exposed to shADP5 solution for 10 min at 37 °C. (c) Samples were then incubated in F/Ca^{2+}/PO_4^{3-} or Ca^{2+}/PO_4^{3-} solutions for 1 h at 37 °C. (d) New mineral layer was characterized structurally and mechanically.

DOI: 10.1021/acsbiomaterials.7b00959
ACS Biomater. Sci. Eng. XXXX, XXX, XXX−XXX

Table 1. Experimental Test Groups and Mineralization Treatments

test groups	treatment	samples
group 1: negative control	no treatment	5
group 2: $Ca^{2+}$and $O4^{3-}$ only	1 h, 4.80 mM Ca^{2+}/2.89 mM PO_4^{3-}	5
group 3: low concentration F	1 h, 1100 ppm F (fluoridated toothpaste concentrations), 4.80 mM Ca^{2+}/2.89 mM PO_4^{3-}	5
group 4: high concentration F	1 h, 20 000 ppm F (dental varnish concentration), then 4.80 mM Ca^{2+}/2.89 mM PO_4^{3-}	5
group 5: shADP5 with low concentration F	(i) 10 min, 0.80 mM peptide (ii) 1 h, 1100 ppm F + 4.80 mM Ca^{2+}/2.89 mM PO_4^{3-}	5
group 6: with peptide, shADP5	(i) 10 min, 0.80 mM peptide (ii) 1 h, 4.80 mM Ca^{2+}/2.89 mM PO_4^{3-}	5

Peptide Design and Synthesis. The peptide shADP5, shortened ADP5, was generated using a procedure that was developed for designing protein-derived peptides, as described previously[31] (see also short synopsis of the procedure in Supporting Information). The peptide (Table 2) was synthesized by using an automated solid-phase

Table 2. Molecular Characteristics of the Peptide shADP5[a]

shADP5 (AA Sequence)*	MW	pI	G.R.A.V.Y.	Charge
SYENSHSQAINVDRT	1720.7	5.30	-1.273	-1

*Color scheme of the amino acids: Small, non-polar: Orange; Hydrophobic: Green; Polar: Magenta; Negatively charged: Red; Positively Charged: Blue.

[a]Color coding of amino acids is according to ref 41.

synthesizer (CS336X; CS-Bio, Menlo Park, CA, United States) through *Fmoc*-chemistry. In this procedure, in the reaction vessel, the Wang resin (Novabiochem, West Chester, PA, United States), was treated with 20% piperidine in DMF to remove the preloaded *Fmoc* group. Next, the incoming side chain protected amino acid was activated with HBTU (Sigma-Aldrich, St Louis, MO, United States) in dimethylformamide (DMF, Sigma-Aldrich) and then transferred into the vessel where it was incubated with the resin for 45 min. After the resin was washed with DMF, this protocol was applied for the addition of each of the next amino acids, and synthesis reaction was monitored by UV absorbance at 301 nm. Following synthesis, the resulting resin-bound peptides were cleaved and the side-chain deprotected using reagent-K [TFA:thioanisole:H_2O:phenol:ethanedithiol (87.5:5:5:2.5), Sigma-Aldrich] and precipitated by cold ether. Crude peptides were purified by RP-HPLC with up to >98% purity (Gemini 10u C18 110A column). The sequence of the peptides was confirmed by a MALDI-TOF mass spectrometry with reflectron (RETOF-MS) on an Autoflex II (Bruker Daltonics, Billerica, MA, United States).

Remineralization Protocol. Prior to remineralization, samples requiring peptide treatments (groups 5 and 6) were incubated in 50 μL of 0.8 mM peptide dissolved in 50 mM Tris buffer solution (TBS) (pH 7.4) for 10 min at 37 °C. Next, treatment samples were placed into 800 μL of 50 mM TBS containing Ca^{2+}/PO_4^{3-} (groups 2 and 5) or $Ca^{2+}/PO_4^{3-}/F^-$ (groups 3, 4, and 6) at concentrations as listed in Table 1 for 1 h at 37 °C and then rinsed with deionized (DI) water, dried by forced air, and stored at room temperature until characterization.

Sample Characterization by SEM and EDXS Analyses: Imaging and Elemental Composition. After remineralization experiments were completed, secondary electron imaging (SEI) in the scanning electron microscope (SEM) was used to characterize the surface morphology and to show the thickness of newly formed mineral layer in cross sections where applicable. Specimen preparation for SEM involved cutting a notch on the back side using a low speed saw (IsoMet, Buehler, Lake Bluff, IL, United States) before they were subjected to WSL formation and remineralization as described above. After the remineralization step was completed, specimens were rinsed with DI water, air-dried gently (<5 PSI), then carefully fractured into 2 pieces along the notch. One of the fractured pieces was mounted on a SEM stub with the mineralizing surface facing up for imaging the surface morphology, and the second piece was mounted with the cross-section facing up to show the thickness of the mineral layer. Mounted specimens were then stored in vacuum for at least 2 h to remove residual moisture, which were then sputter coated with 5 nm-thick platinum (SPI-Sputter Module Coater, SPI Supplies, West Chester, PA, United States). SEM characterization was performed using an FEI Sirion microscope (Sirion, FEI, Hillboro, OR, United States) operating at 10 keV acceleration voltage. The chemical composition was measured by an onboard energy dispersive X-ray spectroscopy (EDXS) system (X-Max^N Si drift detector with AZtecEnergy software package, Oxford Instruments, Abingdon, Oxfordshire, UK). The measurements for each group were pooled from five specimens per group. The average values and standard deviations were calculated and expressed as the mean ± standard error. Possible mineral phases were deduced from these EDXS measurements. It should be noted that given the energy resolution of the instrument and topographical variations, precision of the EDXS measurements was >2%.

Structural Characterization by Transmission Microscopy (TEM). After remineralization steps were completed, TEM samples were collected by carefully shaving off the topmost surface of the remineralized layer from the artificially created white spot lesion using a clean razor blade. The shaved particles were suspended in 100% ethanol, and the suspension was drop-casted onto a carbon coated TEM grid, which was then vacuum-dried before TEM characterization. TEM bright field imaging (BF) imaging and selected areas diffraction were carried out using an FEI Tecnai (FEI, Hillboro, OR, United States) operating at 200 keV.

Mechanical Properties Characterization. Similar to SEM specimen preparation, tooth samples were notched from the back of tooth before remineralization, then fractured along the notch. The specimens were then mounted in a room temperature-cure epoxy, and the cross-section of the fracture was polished to 0.1 μm finish using diamond lapping films (Allied High Tech Products Inc., Rancho Dominguez, CA, United States). Nanoindentation measurements were made using a Triboindentor nanoindentation system (Hysitron Inc., Minneapolis, MN, United States) in air. Hardness (H) and elastic modulus (E_r) were determined by the software accompanying the nanoindentation unit (see Supporting Information).[42−44] To obtain the values that were not indentation volume dependent, maximum indentation depth for all measurements kept at 120 ± 10 nm. All reported H and E_r values were averaged over 20 measurements.

In addition to nanoindentation measurements, microhardness testing was also performed on the surface to quantitatively assess the mechanical properties of the mineral layers with larger areas and volumes including the underlying enamel as a composite. Vicker's microhardness was performed at room temperature using Vicker's indenter on a Wilson Hardness Tukon 1202 microhardness tester at 10 kg applied load (Illinois Tool Works, Lake Bluff, IL). At least 20 measurements per group were recorded for obtaining an average and statistical analysis.

RESULTS

The incubation of samples in demineralization cocktail exposed enamel rods on the surface of the samples before the remineralization treatment was undertaken, as shown in group 1, negative control (Figures 2a and b). Elemental compositional analysis of the surface by EDXS gives a ratio of Ca^{2+}/PO_4^{3-} 1.56 ± 0.12 (Figure 2c). As seen in the cross-sectional view of (Figure 2d), well-aligned enamel rods of ∼3 μm diameter extend to the exposed surface where they display HAp crystallites constituting the rods. After 1 h of exposure to

DOI: 10.1021/acsbiomaterials.7b00959
ACS Biomater. Sci. Eng. XXXX, XXX, XXX−XXX

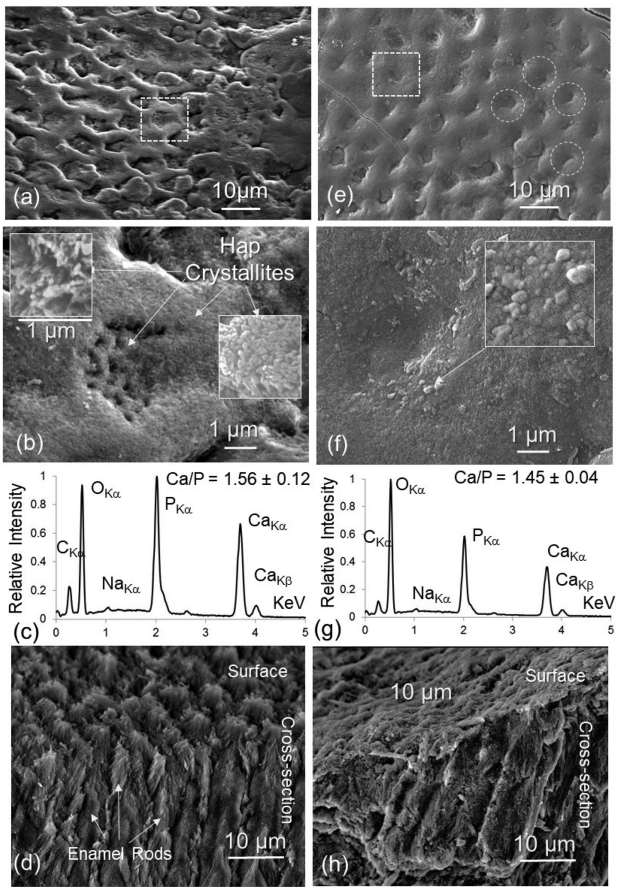

Figure 2. Face-on (a and b) and edge-on (d) SEM images and EDXS analyses (c) of group 1. Face-on (e and f) and edge-on (h) SEM images and EDXS analysis (g) of group 2: Ca^{2+} and PO_4^{3-} only. Insets in b and f show enamel rods and HAp crystallites exposed on the surface of damaged enamel as a result of demineralization. The inset panels are 1 × 1 μm.

Ca^{2+}/PO_4^{3-} solution, no substantial remineralization was observed on the samples in group 2. Considering that the imprints of enamel rods remained visible as shallow depressions on the enamel surface (delineated with circles, Figures 2e and f), any possible deposit of solid material, possibly the result of Ca^{2+} and PO_4^{3-} ions reacting to form an amorphous deposit, remained extremely thin. In fact, a very thin ($\ll$1 μm) layer is barely visible in the SEM image of the cross-sectioned sample shown in Figure 2h. Elemental analysis of the surface by EDXS gives a ratio of Ca^{2+}/PO_4^{3-} 1.45 ± 0.04, possibly indicating a mixed mineral composition (Figure 2g; also see Table 3).

In group 3 (low concentration fluoride), 1100 ppm F was applied in the presence of Ca^{2+} and PO_4^{3-} ions. The concentration of 1100 ppm fluoride corresponds to the concentration of the most commonly used toothpaste available over the counter for daily home care.[5−7] The analysis of the SEM images suggests nonuniformly deposited layer with a fine (<1 μm) roughness (Figures 3a and b). A detailed analysis of

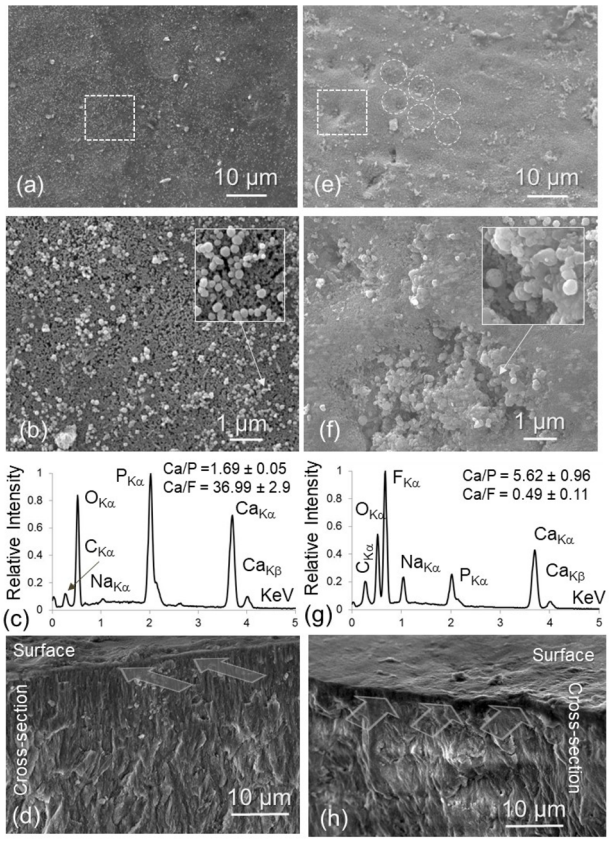

Figure 3. Face-on (a and b) and edge-on (d) SEM images and EDXS analysis (c) of group 3, 1100 ppm F^- + Ca^{2+}/PO_4^{3-}. Face-on (e and f) and edge-on (h) SEM images and EDXS analysis (g) of group 4, 20 000 ppm F + Ca2+/PO43−. Insets in b and f show loosely packed nanospherical particles (of diameter ∼20−30 nm) as a result of F deposition. The inset panels are 1 × 1 μm. Wide arrows in panels d and h indicate the boundary between the new layer and original tooth surface.

the surface structure, e.g., at higher magnification image in Figure 3b, reveals fine nanoparticles of diameter 20−50 nm. The cross-sectioned samples reveal a new layer with a thickness of about 1 μm covering the surface of enamel in the lesion (Figure 3d). The elemental composition analysis from the surface revealed prominent peaks of $O_{K\alpha}$, $P_{K\alpha}$, and $Ca_{L\alpha}$ as well as a small peak corresponding to $F_{K\alpha}$. The Ca/F ratio gives a

Table 3. Elemental Composition Analyses of the Remineralization Test Groups by EDXS

	remineralized layer			possible mineral
test group	Ca/P	Ca/F	Ca/O	formed
1: control	1.56 ± 0.12		0.51 ± 0.11	only HAp
2: ions only	1.45 ± 0.04		0.28 ± 0.02	amorphous Ca−P transition phase
3: low F	1.69 ± 0.05	36.99 ± 2.9	0.74 ± 0.15	Ca−P−F transition phase + CaF_2
4: high F	5.62 ± 0.96	0.49 ± 0.11	1.01 ± 0.16	mainly CaF_2
5: low F + peptide	1.60 ± 0.11	8.74 ± 0.78	0.34 ± 0.08	FAp + some CaF_2
6: peptide only	1.54 ± 0.12		0.56 ± 0.13	only HAp

DOI: 10.1021/acsbiomaterials.7b00959
ACS Biomater. Sci. Eng. XXXX, XXX, XXX−XXX

values of more than 30, while the Ca/P ratio is close to 1.70 (Figure 3c).

In group 4 (high concentration fluoride), 20 000 ppm fluoride (concentrations of most commonly used dental varnishes) applied with Ca^{2+} and PO_4^{3-} ions.[5−7] The analysis of the SEM images recorded from this treatment displayed significantly different surface topography, structures, and elemental composition as compared to the samples in the previous groups of nonfluoride or low concentration F treatment. Although at low magnifications (Figure 3e) the surface appears fairly smooth, higher magnification (Figure 3f) revealed small spherical particles of 100−200 nm diameter covering the overall surface (indicated by arrow in Figure 3f). The secondary electron images, recorded with the SEM, from the cross-sectioned samples reveal an about a micrometer-thick new layer on the surface of the teeth (Figure 3h). The EDXS spectra acquired from the surface gives a high concentration of $F_{K\alpha}$ peak, the most prominent among all the peaks in the spectra from this group of samples (Figure 3g). The quantitative analysis of the spectra from the samples prepared in this group exhibited the Ca/F ratio of 0.49 (Table 3).

In group 5 (the peptide with low concentration fluoride), shADP5 was applied with 1100 ppm fluoride along with Ca^{2+} and PO_4^{3-}. The microstructure of the samples displays fairly smooth surface with about 1−2 μm thickness (Figures 4a−d). Enamel rod imprints remained visible in the lower magnification image (Figure 4a). Higher magnification image of the sample surface, however, exhibits two different surface morphologies (see insets in Figure 4b): somewhat loosely deposited nanoparticles of 50−100 nm diameter and dense structure composed of rod-like nanoparticles of few tens of nanometers in diameters with the diameter/length aspect ratio of 1/5. Elemental analysis of the samples from this group revealed fairly noticeable $F_{K\alpha}$ peak in addition to highly prominent $Ca_{K\alpha}$ and $P_{K\alpha}$ peaks with the elemental ratio of Ca/F, 8.7 (Figure 4c).

In group 6 (shADP5 + Ca^{2+}/PO_4^{3-}), the SEM images in Figures 4e and f give a continuous layer of plate-like crystals growing from the surface of the underlying enamel lesion when the surface is exposed to aqueous peptide plus Ca^{2+}/PO_4^{3-}. Compared to the negative control (group 1) or low concentration fluoride treatment (group 3), the enamel rod imprints in the face-on images are no longer visible, indicating that the new mineral layer is thick enough to mask the previously exposed enamel rods (Figures 4e and f). The cross-sectional image in Figure 4h shows a 10 μm-thick continuous remineralized layer with fairly smooth surface topography. Elemental analysis of the samples from this group revealed prominent $Ca_{K\alpha}$ and $P_{K\alpha}$ peaks with a ratio of 1.54 ± 0.12; this is close to ideal ionic ratio of 1.6 in HAp composition (Figure 4g; Table 3).

To further analyze the structural characteristics of the mineral layers, imaging and diffraction analyses were also carried out on all samples by using transmission electron microscopy (Figure 5 and Figure S2, see Supporting Information). The TEM samples were prepared by gently shaving fragments off the surface of tooth specimens. Group 1 received no mineralization treatment, and the enamel fragments were analyzed. As shown in Figures 5a−c, textured, elongated HAp crystals of 30−50 nm were encountered, typical of prismatic rods constituting the enamel rods in healthy enamel tissue. In the case of high concentration F treatment (group 4), generally round particles CaF_2 in the range of 100−250 nm in

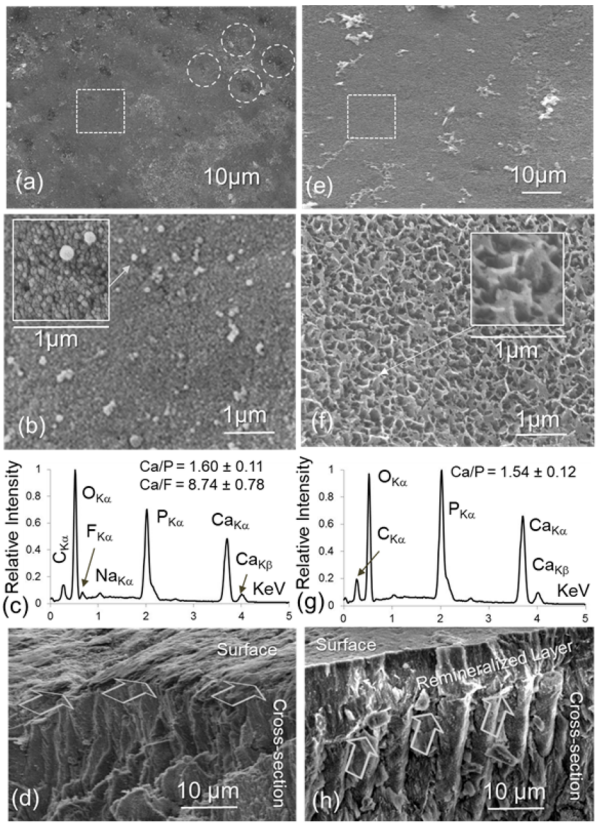

Figure 4. Face-on (a and b) and edge-on (d) SEM images and EDXS analyses (c) of group 5, shADP5 + 1100 ppm F^- + Ca^{2+}/PO_4^{3-}. Insets in b show loosely crystallized regions of accumulated 100 nm diameter spherical nanoparticles on the surface. Face-on (e and f) and edge-on (h) SEM images and EDXS analysis (g) of group 6, shADP5 + Ca^{2+}/PO_4^{3-}. Inset f displays a highly uniform, plate-like HAp crystallites within newly formed (h) mineral layer in shADP5 + Ca^{2+}/PO_4^{3-} treatment. The inset panels are 1 × 1 μm. Wide arrows in panels d and h indicate the boundary between the new layer and original tooth surface.

diameter were observed (Figures 5d−f). On the peptide treatment group (group 6), particles (in the shown projection) of HAp were found (Figures 5g−i), possibly corresponding to plate-shape mineral. It is noted that groups 2, 3, and 5 had structural characteristics similar to those of group 1 in that the mineral had morphological characteristics similar to those of enamel crystallites (data not shown here, but given in the Supporting Information). In all cases, it was challenging but not impossible (as demonstrated in Figure 5 above) to differentiate the newly formed crystallites from the HAp crystallites present in the underlying enamel.

Mechanical properties of the mineralized layers were determined using two different tests. The microhardness test was carried out using a Vicker's indenter loading on the mineralized tooth surface. The hardness for the negative control group (group 1) was 128 ± 8 HV10, which was used as the baseline figure representing microhardness of the surface of bare, artificially created WSL against which other experimental groups compared. As further reference, the microhardness tests were also conducted on healthy enamel and dentin, away from the demineralized surface (Table 4). The values for groups 2−5 ranged between 130 ± 12 HV10 to 134 ± 12 HV10. Unequal variance t test between group 1 and each of other groups revealed no statistically significant difference ($p > 0.05$). The

DOI: 10.1021/acsbiomaterials.7b00959
ACS Biomater. Sci. Eng. XXXX, XXX, XXX−XXX

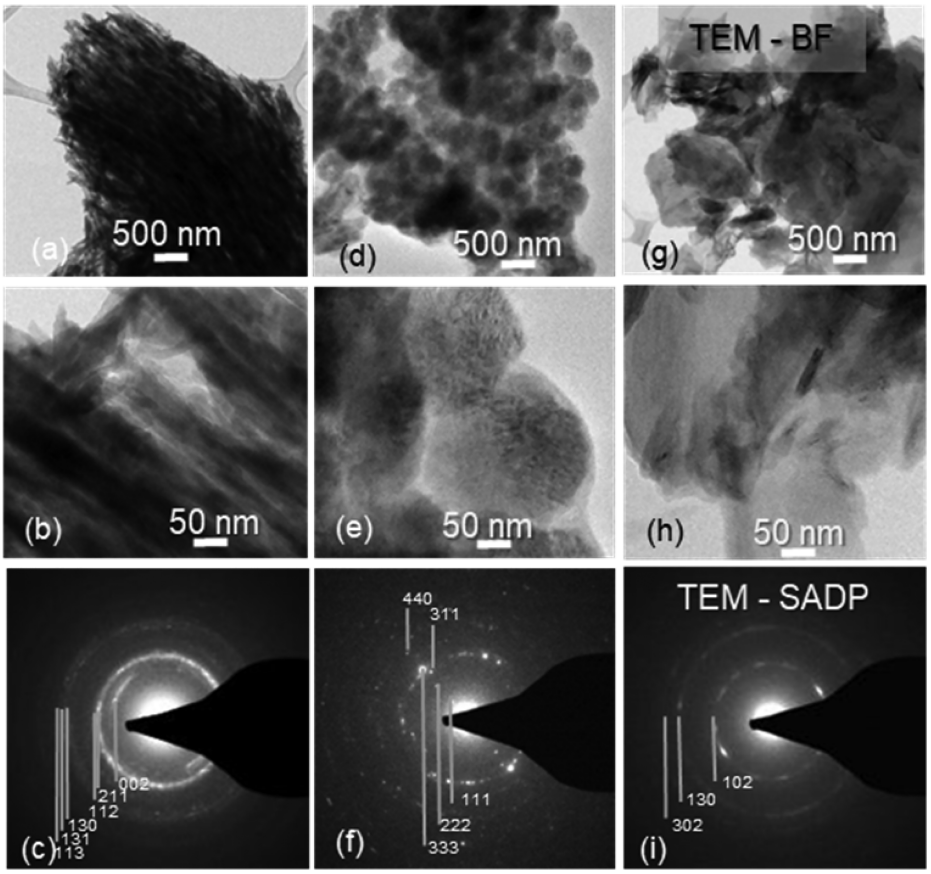

Figure 5. TEM bright field images and corresponding selected diffraction patterns for no-treatment negative control (group 1) (a–c), showing high-aspect ratio rod-like HAp crystallites; high concentration F treatment (group 4) (d–f), exhibiting CaF_2 particles; and peptide-treatment (group 6) (g–i), showing plate-like HAp crystallite formation.

Table 4. Vicker's Microhardness of All Experimental Groups, $n \geq 20$

test group	hardness (HV10, MPa)	STDEV (MPa)
group 1: negative control	128.1	8.0
group 2: Ca/PO4 only	130.1	11.7
group 3: low conc F	130.6	12.6
group 4: high conc F	131.8	12.9
group 5: shADP5 + low conc F	133.5	12.4
group 6: shADP5	141.1	7.8
healthy enamel	290.6	20.1
healthy dentin	63.1	3.0

microhardness values of group 6 had slightly higher average value of 141 ± 8 HV10. Unequal variance *t* test against group 1 revealed significant difference with $p \ll 0.01$. The results indicate that the microhardness values of group 6 as well as the rest of experimental groups fell between that of enamel and dentin.

Nanomechanical tests were also conducted using nanoindentation that not only provided hardness (H) but also elastic modulus (E_r) values, and the tests were carried out in spatially selected regions as the test facilitates scanned surface images. The nanoindentation tests of all the experimental groups were conducted on samples in cross-sectional geometry, i.e., indentor direction being parallel to the surface (as opposed to vertical in microhardness tests) (Figure S1a). The results (Figure 6) reveal a trend similar to the those of the microhardness data; no significant differences were encountered among the samples from the no-treatment negative control and each of the groups 2 through 5 in both hardness and reduced elastic modulus, $p > 0.05$ in all cases. However, the average hardness and elastic modulus for group 6 were higher than those of the no-treatment samples with hardness of 2.23 ± 0.23 GPa vs 2.10 ± 0.26 GPa, $p = 0.02$ and elastic modulus of 58.6 ± 4.7 GPa vs 55.1 ± 4.3 GPa, $p = 0.02$. Not surprisingly, the healthy enamel and dentin had, respectively, higher and lower values of both hardness and elastic moduli compared to the experimental groups involving remineralization. In conclusion, the mechanical properties (H and E) are higher than those of dentin but lower than those of the healthy enamel.

DISCUSSION

A natural, cell-free, biomimetic model was developed to remineralize artificially induced lesions on human enamel using a 15-amino acid long amelogenin-derived peptide, shADP5, along with properly tuned ionic concentrations of Ca^{2+}/PO_4^{3-} in vitro in the presence and absence of low and high fluoride content that were chosen based on the values in the frequently used current dental treatments. Significant differences were encountered among the surface characteristics of the samples from six different groups of tests. The surface of the artificially demineralized enamel displayed enamel rods, and up to 3-μm diameter depressions exposed on the surface appeared (Figures 2a and b) with a roughness of approximately 1 μm. Another prominent feature was the fine structure of the individual rod-shaped HAp crystallites of a few tens of nanometers in thickness that constitute the enamel rods.

DOI: 10.1021/acsbiomaterials.7b00959
ACS Biomater. Sci. Eng. XXXX, XXX, XXX–XXX

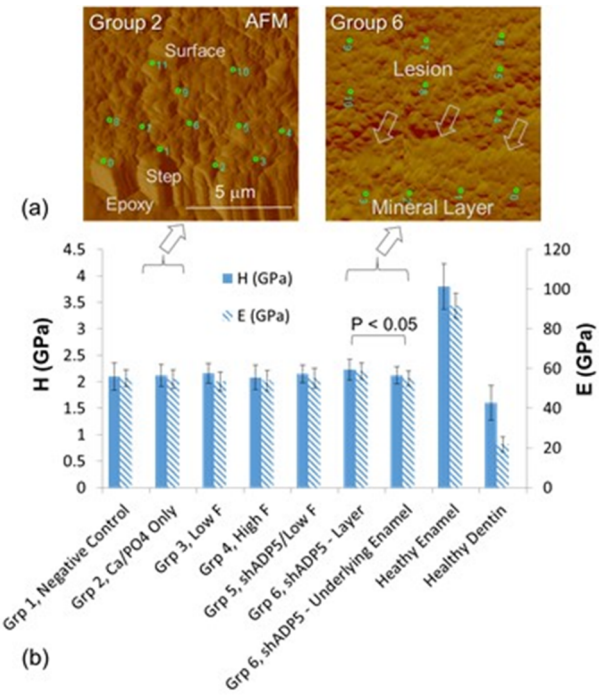

Figure 6. (a) Atomic force microscopy images of the surfaces of the mineralized layers in samples from group 2 (left), where there is no apparent mineral layer on the lesion, and group 6 (right), showing a clear boundary between the lesion and newly formed mineral layer (arrows). (b) Hardness (left) and elastic modulus (right) of the experimental groups used here were measured by nanoindentation, $n > 20$.

When ionic precursors are used alone (group 2), the treatment resulted in a thin (<1 μm) layer with a highly porous morphology on the surface. The composition was off-stoichiometric for that of HAp, with Ca/P ratio of <1.5, possibly due to the formation of calcium-phosphate transition phases (Table 3 and Table S1). The effect of F on mineral formation was examined under 2 different fluoride ion conditions, 1100 ppm in group 3 and 20 000 ppm in group 4, specifically chosen to mimic the F concentrations of the usual over-the-counter toothpaste and clinical fluoride varnish, respectively. The surface structures of the teeth in these two treatments revealed different morphologies. First, F treatments resulted in aggregates of nanoparticles in group 3, and a thin mineralized layer of about 1 μm in group 4. The layers were composed of nanoparticles which were about an order of magnitude smaller in group 3 than in group 4 samples, ~20 nm versus ~200 nm, respectively. The application of F in dental care products primarily focuses on remineralization, aided by F or incorporation of F into the existing HAp structure, desirably forming FAp. In this respect, the results of the elemental analyses obtained from the fluoride-treated surfaces are quite intriguing. The group 3 samples (low-F) presented hardly any F-peaks in the EDXS spectra, giving Ca/F ratio of almost 40. The elemental composition analysis of the sample surface displayed relatively strong peaks of $O_{K\alpha}$, $P_{K\alpha}$, and $Ca_{L\alpha}$ as well as a minor peak corresponding to $F_{K\alpha}$ ($Na_{K\alpha}$ and $Cl_{L\alpha}$ peaks are from the treatment solutions). Possible sources of the low F concentration might be explained either as being due to the formation of a very thin newly deposited layer in the signals mainly originating from the underlying healthy enamel, as determined EDXS, or due to the very low amount of F incorporated into the newly formed surface layer. The concentration in the newly formed layer may imply that majority of F was not delivered to the desired mineralization site on the tooth surface in the peptide-free samples. The presence of nanoparticles deposited on the surface, therefore, may be due to F reacting with the excess Na in the buffer solution forming NaF.

In group 4, the new layer is predominantly composed of aggregated spherical nanoparticles. Considering the ideal Ca/F ratio of 0.5 in CaF_2 (Table S1, Supporting Information, and Figures 5d–f, TEM results), the spherical particles are likely to be CaF_2. Another major difference in this group was the value of $Ca_{K\alpha}/P_{K\alpha}$ ratio being >5.0. Even considering that some of the Ca ions might be confined to CaF_2, this ratio still indicates unusually high concentration of Ca trapped in the newly formed surface layer. Calcium fluoride is a highly stable compound, likely to form under the experimental conditions used in this study. The clinical products that contain high F concentration are designed for forming apatite in the demineralized product. However, as shown here, the mineral formed is most likely calcium fluoride. In summary, neither of the F samples exhibited the ideal ratio of Ca/P of 1.6 for HAp (Table 3), meaning that F alone was not incorporated into the enamel or remineralized layer. These findings are consistent with previous studies that reported CaF_2 formation under home-use (low-F) and clinical (high-F) products.[45−47] It has been suggested that CaF_2 may serve as a reservoir of fluoride, presumably, to be incorporated later into the structure of enamel.[47−49]

In groups 5 and 6, the peptide was used as the precursor in the remineralization procedure. In group 5, shADP5 was applied in the presence of 1100 ppm fluoride, resulting in the formation of the spherical particles as aggregates as opposed to being widely disseminated on the tooth surface compared to the same F concentration without peptide in group 3. Enamel rod imprints remained visible in the lower magnification image (Figures 4a and b), although these were less prominent than those seen in the no-treatment samples (Figures 2a and b). The resulting mineralized structure presented two morphologies: clusters of 50−100 nm diameter spherical nanoparticles accrued nonuniformly on the surface, and a structure primarily composed of highly dense nanorods. There was a considerably more prominent F peak compared to the no-peptide samples, with an overall Ca/F ratio of 8.74 ± 0.78. This explains that there was considerably more F in the mineral formed with the peptide containing low-fluoride treatment compared to the samples with low-fluoride only (Ca/F = 36.99 ± 2.9). If the presence of FAp is considered, i.e., corresponding to the dense nanorods, the ideal ratio of Ca/F turns out to be 5.0 (Table 3), then the rest of the fluoride in the mineral layer could be accounted for the formation of NaF nanoparticles. Considering that the observed Ca/P ratio reflects either HAp or FAp stoichiometry (Table 3), the new mineral was formed on the teeth surface by partially incorporating F in the presence of peptide. The presence of F could be explained in at least two ways: either the fluoride was incorporated into the newly forming HAp mineral replacing OH partially, or both HAp and FAp were formed on the surface. In both cases, the effect of peptide appears to be necessary to incorporate fluoride into the structure because in the absence of shADP5, very little or no F was found in the remineralized layer. The significance here is that dental formulations used in the current treatments, e.g., pastes, gels, varnish, and solutions, could contain peptide as a

DOI: 10.1021/acsbiomaterials.7b00959
ACS Biomater. Sci. Eng. XXXX, XXX, XXX−XXX

means to effectively carry F to the surface and help incorporate it into the remineralized HAp on the tooth surface.

In group 6, shADP5 peptide in addition to calcium and phosphate precursors were used which remineralized a thick (>10 μm) layer composed of crystal morphology specific to HAp among the calcium phosphate polymorphs. Considering that he observed Ca/P ratio is 1.54, close to that of ideal HAp composition, it is concluded that the peptide was capable to catalyze a newly mineralized layer composed of HAp crystallites (Figures 5g–i). As evident from SEM images (Figures 4e–f), the roughness of remineralized surface was reduced (<300 nm) compared to the demineralized surface in group 1 (Figures 2a, b, and d).

The loading in the microhardness tests were carried out in the direction relevant to functional dentition loading while using the lowest possible Vicker's indentation load to maximize the contribution from the mineralization layer. Even with the lowest load, however, the indentor likely penetrated through the thin mineralized layers in the samples from groups 2–5 as no discernible measurements were determined among these groups compared to the no-treatment negative control group. The SEM observations supported these findings as the mineral layers in groups 2–5 were significantly thinner (~1–2 μm or less) and discontinuous. The remineralized layer, however, was thicker in peptide-guided remineralized group, reflected in higher microhardness values, although slight, compared to the negative control group.

CONCLUSIONS

The present in vitro study demonstrated that crystalline mineral layer is formed on an artificially created lesion on human enamel in the presence of Ca^{2+} and PO_4^{3-} ions under physiologically viable conditions by using shADP5, a 15-AA long amelogenin-derived peptide. This study also showed that the presence of biomineralizing peptide also facilitated the delivery to tooth surface and incorporation of fluoride ions into the remineralized layer even at low F concentrations, providing an opportunity for dental health products to incorporate both elements in potential clinical and everyday dental product formulations.

Establishing the scientific foundations for remineralization has a high potential to empower practicing dentists to address caries-related dental problems due to enamel demineralization, the origin of most dental ailments. Although remineralization on human teeth in vitro using peptides on artificially damaged enamel discussed herein provides guidance toward addressing this challenge, the procedures developed need to be further optimized toward clinical applications. Further research concerning the repair of enamel defects is necessary to achieve an easy-to-apply, fast-growing enamel-like biomineralized tissue for biomimetic tooth repair. Future studies (underway in the authors' laboratories) include implementing this advanced remineralization technology under in vivo conditions by utilizing clinically applicable peptide delivery systems (e.g., gels or pastes with or without F) and applying tests to the mineralized layer to ensure its mechanical and chemical durability and adherence to the underlying tooth structure.

ASSOCIATED CONTENT

Supporting Information

The Supporting Information is available free of charge on the ACS Publications website at DOI: 10.1021/acsbiomaterials.7b00959.

Detailed description of the design of amelogenin-derived peptides; a list of calcium, phosphate, fluoride, and oxygen containing minerals with the calculated elemental composition ratios; TEM studies of the samples from all six test groups; and comparison of microhardness testing and nanoindentation plus a table of hardness and elastic modulus values from nanoindentation tests (PDF)

AUTHOR INFORMATION

Corresponding Author

*Phone: 206-543-0724; Fax: 206-543-3100; E-mail: sarikaya@u.washington.edu.

ORCID

Mehmet Sarikaya: 0000-0003-3856-6360

Notes

The authors declare no competing financial interest.

ACKNOWLEDGMENTS

This research was mainly supported (D.T.Y., H.F., M.S.) by WA-LSDF (Washington State Life Sciences Discovery Funds) and also by NSF through MGI/DMREF program (DMR-1629071) at GEMSEC, Genetically Engineered Materials Science and Engineering Center (D.T.Y., M.S.). S.D., G.H., and T.C. were supported by Spencer Fund (Restorative Dentistry, University of Washington); D.T.Y. was also supported by TC-Education Ministry Fund, and S.D. by NIDCR T32. The work was carried out at the GEMSEC-SECF, a member of Materials Facilities Network of MRSEC.

REFERENCES

(1) Selwitz, R. H.; Ismail, A. I.; Pitts, N. B. Dental caries. *Lancet* **2007**, *369*, 51–59.

(2) Gorelick, L.; Geiger, A. M.; Gwinnett, A. J. Incidence of white spot formation after bonding and banding. *Am. J. Orthod.* **1982**, *81*, 93–98.

(3) Featherstone, J. D. The science and practice of caries prevention. *J. Am. Dent. Assoc., JADA* **2000**, *131*, 887–899.

(4) Huang, Z.; Newcomb, C. J.; Bringas, P., Jr; Stupp, S. I.; Snead, M. L. Biological synthesis of tooth enamel instructed by an artificial matrix. *Biomaterials* **2010**, *31*, 9202–9211.

(5) American Dental Association Council on Scientific, A. Professionally applied topical fluoride: Evidence–based clinical recommendations. *J. Am. Dent. Assoc., JADA* **2006**, *137*, 1151–1159.

(6) Ammari, A. B.; Bloch-Zupan, A.; Ashley, P. F. Systematic review of studies comparing the anti-caries efficacy of children's toothpaste containing 600 ppm of fluoride or less with high fluoride toothpastes of 1,000 ppm or above. *Caries Res.* **2003**, *37*, 85–92.

(7) Petersson, L. G.; Twetman, S.; Dahlgren, H.; Norlund, A.; Holm, A. K.; Nordenram, G.; Lagerlof, F.; Soder, B.; Kallestal, C.; Mejare, I.; Axelsson, S.; Lingstrom, P. Professional fluoride varnish treatment for caries control: a systematic review of clinical trials. *Acta Odontol. Scand.* **2004**, *62*, 170–176.

(8) Cate, J. M. Review on fluoride, with special emphasis on calcium fluoride mechanisms in caries prevention. *Eur. J. Oral Sci.* **1997**, *105*, 461–465.

(9) Al-Mullahi, A. M.; Toumba, K. J. Effect of slow-release fluoride devices and casein phosphopeptide/amorphous calcium phosphate nanocomplexes on enamel remineralization in vitro. *Caries Res.* **2010**, *44*, 364–371.

(10) Krithikadatta, J.; Fredrick, C.; Abarajithan, M.; Kandaswamy, D. Remineralisation of occlusal white spot lesion with a combination of 10% CPP-ACP and 0.2% sodium fluoride evaluated using Diagnodent: a pilot study. *Oral Health Prev Dent* **2013**, *11*, 191–196.

DOI: 10.1021/acsbiomaterials.7b00959
ACS Biomater. Sci. Eng. XXXX, XXX, XXX–XXX

(11) Meyer-Lueckel, H.; Wierichs, R. J.; Schellwien, T.; Paris, S. Remineralizing efficacy of a CPP-ACP cream on enamel caries lesions in situ. *Caries Res.* **2015**, *49*, 56−62.
(12) Rølla, G.; Saxegaard, E. Critical Evaluation of the Composition and Use of Topical Fluorides, with Emphasis on the Role of Calcium Fluoride in Caries Inhibition. *J. Dent. Res.* **1990**, *69*, 780−785.
(13) Sitthisettapong, T.; Phantumvanit, P.; Huebner, C.; Derouen, T. Effect of CPP-ACP paste on dental caries in primary teeth: a randomized trial. *J. Dent. Res.* **2012**, *91*, 847−852.
(14) Vanichvatana, S.; Auychai, P. Efficacy of two calcium phosphate pastes on the remineralization of artificial caries: a randomized controlled double-blind in situ study. *Int. J. Oral Sci.* **2013**, *5*, 224−228.
(15) Wong, M. C.; Clarkson, J.; Glenny, A. M.; Lo, E. C.; Marinho, V. C.; Tsang, B. W.; Walsh, T.; Worthington, H. V. Cochrane reviews on the benefits/risks of fluoride toothpastes. *J. Dent. Res.* **2011**, *90*, 573−579.
(16) Balakrishnan, M.; Simmonds, R. S.; Tagg, J. R. Dental caries is a preventable infectious disease. *Aust. Dent. J.* **2000**, *45*, 235−245.
(17) Featherstone, J. D. The caries balance: the basis for caries management by risk assessment. *Oral Health Prev Dent* **2004**, *2*, 259−264.
(18) Yamagishi, K.; Onuma, K.; Suzuki, T.; Okada, F.; Tagami, J.; Otsuki, M.; Senawangse, P. Materials chemistry: a synthetic enamel for rapid tooth repair. *Nature* **2005**, *433*, 819.
(19) Huang, S.; Gao, S.; Cheng, L.; Yu, H. Remineralization potential of nano-hydroxyapatite on initial enamel lesions: an in vitro study. *Caries Res.* **2011**, *45*, 460−468.
(20) Ingram, G. S.; Silverstone, L. M. A chemical and histological study of artificial caries in human dental enamel in vitro. *Caries Res.* **1981**, *15*, 393−398.
(21) Koulourides, T.; Cueto, H.; Pigman, W. Rehardening of softened enamel surfaces of human teeth by solutions of calcium phosphates. *Nature* **1961**, *189*, 226−227.
(22) ten Cate, J. M.; Jongebloed, W. L.; Arenas, J. Remineralization of artificial enamel lesions in vitro. IV. Influence of fluorides and diphosphonates on short- and long-term reimineralization. *Caries Res.* **1981**, *15*, 60−69.
(23) Bleek, K.; Taubert, A. New developments in polymer-controlled, bioinspired calcium phosphate mineralization from aqueous solution. *Acta Biomater.* **2013**, *9*, 6283−6321.
(24) Fan, Y.; Sun, Z.; Moradian-Oldak, J. Controlled remineralization of enamel in the presence of amelogenin and fluoride. *Biomaterials* **2009**, *30*, 478−483.
(25) Fowler, C. E.; Li, M.; Mann, S.; Margolis, H. C. Influence of surfactant assembly on the formation of calcium phosphate materials - A model for dental enamel formation. *J. Mater. Chem.* **2005**, *15*, 3317−3325.
(26) Kirkham, J.; Firth, A.; Vernals, D.; Boden, N.; Robinson, C.; Shore, R. C.; Brookes, S. J.; Aggeli, A. Self-assembling peptide scaffolds promote enamel remineralization. *J. Dent. Res.* **2007**, *86*, 426−430.
(27) Li, Q. L.; Ning, T. Y.; Cao, Y.; Zhang, W. B.; Mei, M. L.; Chu, C. H. A novel self-assembled oligopeptide amphiphile for biomimetic mineralization of enamel. *BMC Biotechnol.* **2014**, *14*, 32.
(28) Ruan, Q.; Zhang, Y.; Yang, X.; Nutt, S.; Moradian-Oldak, J. An amelogenin-chitosan matrix promotes assembly of an enamel-like layer with a dense interface. *Acta Biomater.* **2013**, *9*, 7289−7297.
(29) Shafiei, F.; Hossein, B. G.; Farajollahi, M. M.; Fathollah, M.; Marjan, B.; Tahereh, J. K. Leucine-rich amelogenin peptide (LRAP) as a surface primer for biomimetic remineralization of superficial enamel defects: An in vitro study. *Scanning* **2015**, *37*, 179−185.
(30) Wu, D.; Yang, J.; Li, J.; Chen, L.; Tang, B.; Chen, X.; Wu, W.; Li, J. Hydroxyapatite-anchored dendrimer for in situ remineralization of human tooth enamel. *Biomaterials* **2013**, *34*, 5036−5047.
(31) Gungormus, M.; Oren, E. E.; Horst, J. A.; Fong, H.; Hnilova, M.; Somerman, M. J.; Snead, M. L.; Samudrala, R.; Tamerler, C.; Sarikaya, M. Cementomimetics-constructing a cementum-like biomineralized microlayer via amelogenin-derived peptides. *Int. J. Oral Sci.* **2012**, *4*, 69−77.
(32) Oren, E. E.; Tamerler, C.; Sahin, D.; Hnilova, M.; Seker, U. O.; Sarikaya, M.; Samudrala, R. A novel knowledge-based approach to design inorganic-binding peptides. *Bioinformatics* **2007**, *23*, 2816−2822.
(33) Gungormus, M.; Fong, H.; Kim, I. W.; Evans, J. S.; Tamerler, C.; Sarikaya, M. Regulation of in vitro calcium phosphate mineralization by combinatorially selected hydroxyapatite-binding peptides. *Biomacromolecules* **2008**, *9*, 966−973.
(34) Moradian-Oldak, J.; Paine, M. L.; Lei, Y. P.; Fincham, A. G.; Snead, M. L. Self-Assembly Properties of Recombinant Engineered Amelogenin Proteins Analyzed by Dynamic Light Scattering and Atomic Force Microscopy. *J. Struct. Biol.* **2000**, *131*, 27−37.
(35) Paine, M. L.; White, S. N.; Luo, W.; Fong, H.; Sarikaya, M.; Snead, M. L. Regulated gene expression dictates enamel structure and tooth function. *Matrix Biol.* **2001**, *20*, 273−292.
(36) Snead, M. L.; Lau, E. C.; Zeichner-David, M.; Fincham, A. G.; Woo, S. L.; Slavkin, H. C. DNA sequence for cloned cDNA for murine amelogenin reveal the amino acid sequence for enamel-specific protein. *Biochem. Biophys. Res. Commun.* **1985**, *129*, 812−818.
(37) Han, S.; Fan, Y.; Zhou, Z.; Tu, H.; Li, D.; Lv, X.; Ding, L.; Zhang, L. Promotion of enamel caries remineralization by an amelogenin-derived peptide in a rat model. *Arch. Oral Biol.* **2017**, *73*, 66−71.
(38) Hoppenbrouwers, P. M.; Driessens, F. C. The effect of lactic and acetic acid on the formation of artificial caries lesions. *J. Dent. Res.* **1988**, *67*, 1466−1467.
(39) Lynch, R. J. M.; ten Cate, J. M. The Effect of Lesion Characteristics at Baseline on Subsequent De- and Remineralisation Behaviour. *Caries Res.* **2006**, *40*, 530−535.
(40) Naumova, E. A.; Niemann, N.; Aretz, L.; Arnold, W. H. Effects of different amine fluoride concentrations on enamel remineralization. *J. Dent.* **2012**, *40*, 750−755.
(41) Lesk, A. *Introduction to Bioinformatics*; Oxford University Press: Oxford, 2013.
(42) Fong, H.; Sarikaya, M.; White, S. N.; Snead, M. L. Nano-mechanical properties profiles across dentin-enamel junction of human incisor teeth. *Mater. Sci. Eng., C* **1999**, *7*, 119−128.
(43) Gallagher, R. R.; Balooch, M.; Balooch, G.; Wilson, R. S.; Marshall, S. J.; Marshall, G. W. Coupled Nanomechanical and Raman Microspectroscopic Investigation of Human Third Molar DEJ. *J. Dent Biomech* **2010**, *1*, 256903.
(44) Oliver, W. C.; Pharr, G. M. An improved technique for determining hardness and elastic modulus using load and displacement sensing indentation experiments. *J. Mater. Res.* **1992**, *7*, 1564−1583.
(45) Harding, A. M.; Zero, D. T.; Featherstone, J. D.; McCormack, S. M.; Shields, C. P.; Proskin, H. M. Calcium fluoride formation on sound enamel using fluoride solutions with and without lactate. *Caries Res.* **1994**, *28* (1), 1−8.
(46) Petzold, M. The influence of different fluoride compounds and treatment conditions on dental enamel: a descriptive in vitro study of the CaF(2) precipitation and microstructure. *Caries Res.* **2001**, *35*, 45−51.
(47) Cate, J. M. Review on fluoride, with special emphasis on calcium fluoride mechanisms in caries prevention. *Eur. J. Oral Sci.* **1997**, *105* (5 Pt 2), 461−465.
(48) Tenuta, L. M.; Cerezetti, R. V.; Del Bel Cury, A. A.; Tabchoury, C. P.; Cury, J. A. Fluoride release from CaF2 and enamel demineralization. *J. Dent. Res.* **2008**, *87* (11), 1032−1036.
(49) Tenuta, L. M.; Zamataro, C. B.; Del Bel Cury, A. A.; Tabchoury, C. P.; Cury, J. A. Mechanism of fluoride dentifrice effect on enamel demineralization. *Caries Res.* **2009**, *43* (4), 278−285.

DOI: 10.1021/acsbiomaterials.7b00959
ACS Biomater. Sci. Eng. XXXX, XXX, XXX−XXX